



Molecular mechanism underlying selective inhibition of mRNA nuclear export by herpesvirus protein ORF10

Han Feng^{a,b,c,1}, Huabin Tian^{a,b,1}, Yong Wang^{a,b,c}, Qixiang Zhang^{a,b,c,d}, Ni Lin^{a,b,c,d}, Songqing Liu^{a,b,c}, Yang Yu^{b,e}, Hongyu Deng^{a,b,2}, and Pu Gao^{a,b,c,f,2}

^aCAS Key Laboratory of Infection and Immunity, Institute of Biophysics, Chinese Academy of Sciences, Beijing 100101, China; ^bCAS Center for Excellence in Biomacromolecules, Institute of Biophysics, Chinese Academy of Sciences, Beijing 100101, China; ^cCAS Center for Excellence in Biomacromolecules, Institute of Biophysics, Chinese Academy of Sciences, Beijing 100101, China; ^dUniversity of Chinese Academy of Sciences, Beijing 100049, China; ^eKey Laboratory of RNA Biology, Institute of Biophysics, Chinese Academy of Sciences, Beijing 100101, China; and ^fBioland Laboratory (Guangzhou Regenerative Medicine and Health Guangdong Laboratory), Guangzhou Institutes of Biomedicine and Health, Chinese Academy of Sciences, Guangzhou 510320, China

Edited by Yuan Chang, University of Pittsburgh, Pittsburgh, PA, and approved September 10, 2020 (received for review April 22, 2020)

Viruses employ multiple strategies to inhibit host mRNA nuclear export. Distinct to the generally nonselective inhibition mechanisms, ORF10 from gammaherpesviruses inhibits mRNA export in a transcript-selective manner by interacting with Rae1 (RNA export 1) and Nup98 (nucleoporin 98). We now report the structure of ORF10 from MHV-68 (murine gammaherpesvirus 68) bound to the Rae1–Nup98 heterodimer, thereby revealing detailed intermolecular interactions. Structural and functional assays highlight that two highly conserved residues of ORF10, L60 and M413, play critical roles in both complex assembly and mRNA export inhibition. Interestingly, although ORF10 occupies the RNA-binding groove of Rae1–Nup98, the ORF10–Rae1–Nup98 ternary complex still maintains a comparable RNA-binding ability due to the ORF10–RNA direct interaction. Moreover, mutations on the RNA-binding surface of ORF10 disrupt its function of mRNA export inhibition. Our work demonstrates the molecular mechanism of ORF10-mediated selective inhibition and provides insights into the functions of Rae1–Nup98 in regulating host mRNA export.

RNA nuclear export | Rae1 | Nup98 | ORF10 | herpesvirus

Nuclear export of mRNA plays an important role in gene expression, which is critical for all eukaryotic cells in order to respond to cellular stresses and environmental stimuli and to properly regulate growth and proliferation. After transcription, mRNAs must be properly processed into a mature mRNA by undergoing capping, splicing, and polyadenylation, followed by being packaged into a messenger ribonucleoprotein particle (mRNP) (1–3). mRNP recruits mRNA export factors that provide access to the nuclear pore complex (NPC) and allow for their transportation through the NPC central channel (2, 4, 5). The NXF1 (nuclear export factor 1)–NXT1 (NTF2-like export factor 1) heterodimer complex represents the major export factor and mediates export of bulk mRNAs (6–8). The NXF1–NXT1 heterodimer interacts with phenylalanine-glycine (FG) repeats on nucleoporins (Nups), such as Nup98, which mediate the translocation of mRNPs through the NPC (9, 10). Another export factor involved in this process is Rae1 (RNA export 1), a nucleocytoplasmic shuttling protein that facilitates mRNP docking onto Nup98 (11). Given that Rae1 was found to interact with mRNA, NXF1, and Nup98 (11–17), a model has been proposed in which Rae1 functions to promote the recruitment of NXF1 to Nup98. Rae1 and its interacting partner Nup98 have also been suggested to play other important roles in regulating mRNA trafficking; however, the function of the Rae1–Nup98 complex remains only partially understood.

Nuclear export of host mRNA that encodes antiviral factors is critical for antiviral protein production and control of viral replication. It is not surprising that several viruses have evolved sophisticated strategies to inhibit nuclear export of host mRNAs by targeting mRNA export pathways (10, 18). For example, non-structural protein 1 (NS1) from the influenza A virus (IAV) binds to the mRNA export factor NXF1–NXT1 and prevents binding of

NXF1–NXT1 to nucleoporins, thereby inhibiting mRNA export through the NPC (19–22). Another well-studied viral inhibitor is the matrix protein (M) encoded by the vesicular stomatitis virus (VSV). The M protein directly interacts with the Rae1–Nup98 complex and blocks the mRNA-binding groove of Rae1, thus preventing export of bulk mRNAs during VSV infection (15, 17, 23, 24).

In general, the viral inhibition of mRNA export is believed to be unspecific, as exemplified by the NS1 and M proteins. However, a recent study reported that the ORF10 protein from Kaposi's sarcoma-associated herpesvirus (KSHV) or murine gammaherpesvirus 68 (MHV-68) can selectively block nuclear export of a subset of cellular mRNAs based on their 3' UTRs (25). Herpesviruses are large DNA viruses and replicate within the nucleus. Thus, they need to manipulate host cellular mRNA export machineries to facilitate the export of viral transcripts and in the meantime selectively inhibit host mRNA export. For example, the viral RNA-binding protein ICP27 of herpes simplex virus 1 (HSV-1) and its homologs in other herpesviruses directly bind to mRNA export factors, including NXF1, which recruits viral mRNAs to export receptors for preferential transport into the cytoplasm (26–28). On the other hand, ORF10 represents

Significance

Nuclear export of host mRNAs is critical for proper cellular functions and survival. To mitigate this effort, viruses have evolved multiple strategies to inhibit this process. Distinct to the generally nonselective inhibition mechanisms, ORF10 from gammaherpesviruses blocks nuclear export of selective mRNAs by forming a complex with Rae1 (RNA export 1) and Nup98 (nucleoporin 98). Here we determine the structure of the ORF10–Rae1–Nup98 ternary complex and demonstrate that the intermolecular interactions are critical for both complex assembly and mRNA export inhibition. Moreover, we find that the ORF10–RNA direct interaction is important for ORF10-mediated mRNA export inhibition. This work is essential to understand the diversity of viral-mediated mRNA export inhibition and to design potential antiviral therapies.

Author contributions: H.F., H.T., H.D., and P.G. designed research; H.F., H.T., Y.W., Q.Z., N.L., S.L., and P.G. performed research; H.F., H.T., Y.Y., H.D., and P.G. analyzed data; and H.F., H.T., H.D., and P.G. wrote the paper.

The authors declare no competing interest.

This article is a PNAS Direct Submission.

This open access article is distributed under [Creative Commons Attribution-NonCommercial-NoDerivatives License 4.0 \(CC BY-NC-ND\)](https://creativecommons.org/licenses/by-nc-nd/4.0/).

¹H.F. and H.T. contributed equally to this work.

²To whom correspondence may be addressed. Email: hydeng@moon.ibp.ac.cn or gaopu@ibp.ac.cn.

This article contains supporting information online at <https://www.pnas.org/lookup/suppl/doi:10.1073/pnas.200774117/-DCSupplemental>.

First published October 8, 2020.

the first viral protein encoded by the herpesvirus family that blocks the export of certain cellular mRNAs by interacting with the Rae1–Nup98 complex.

Both ORF10 from KSHV/MHV-68 and M protein from VSV target the Rae1–Nup98 complex, highlighting the importance of Rae1–Nup98 in mRNA export. However, these two viral proteins manifest distinct inhibition mechanisms. While the interaction with the M protein abolishes the mRNA-binding ability of Rae1–Nup98 (23), the ORF10–Rae1–Nup98 complex still associates with mRNAs (25). Moreover, ORF10 selectively inhibits the export of a subset of cellular mRNAs (25), while the M protein nonspecifically prevents export of bulk mRNAs (15, 24). Here we determined the crystal structure of ORF10 in a complex with Rae1–Nup98 and conducted extensive biochemical and cellular functional assays, thereby demonstrating the molecular mechanism and structural basis of ORF10-mediated selective inhibition of mRNA export.

Results

In Vitro Assembly and Structure Determination of the ORF10–Rae1–Nup98 Heterotrimer. Previous coimmunoprecipitation (co-IP) and colocalization experiments have shown that ORF10 interacts with the Rae1–Nup98 complex in a cellular context (25). To check whether ORF10 can form stable and direct interactions with Rae1–Nup98 in vitro, we purified the MHV-68 ORF10 and the mouse Rae1–Nup98^{GLEBS} (GLEBS: Gle2/Rae1-binding sequence of Nup98; amino acids [aa] 157 to 213) complex by using a baculovirus–insect cell system. Size exclusion chromatography (SEC) assays show that ORF10 and Rae1–Nup98^{GLEBS} both adopt a monomeric assembly on their own and further form a stable monomeric heterotrimer (ORF10:Rae1:Nup98 = 1:1:1) upon incubation (Fig. 1A and B). To facilitate the crystallization processes, further truncations for ORF10 and Rae1 were designed, and a heterotrimer complex containing the full-length ORF10, the unstructured NTE (N-terminal extension; aa 1 to 23)-deleted Rae1, and the whole GLEBS region of Nup98 successfully crystallized (Fig. 1A). Hereafter, we refer to this crystallized complex simply as the ORF10–Rae1–Nup98 heterotrimer. The structure was determined by the Hg-derivative single-wavelength anomalous diffraction method and refined to a 2.5 Å resolution with good stereochemical parameters (Fig. 1C; detailed crystallographic analyses are summarized in *SI Appendix, Tables S1 and S2*). There are two ORF10–Rae1–Nup98 heterotrimers in the asymmetric unit, and they can be well superimposed on each other (*SI Appendix, Fig. S1 A and B*), indicating a stable assembly of the heterotrimer complex. Given that Hg soaking greatly improves the crystal diffraction and the native and Hg-derivative structures are almost identical (*SI Appendix, Fig. S1C*), hereafter we only focus on the Hg-derivative structure.

Structural Overview of ORF10. The Rae1–Nup98 moiety in the heterotrimer complex adopts a conformation similar to its apo form structure (17) (*SI Appendix, Fig. S1D*). ORF10 resembles an overall L-like shape, with the first three globular domains forming the long stalk and the extended C-terminal tail (CTT) forming the short arm (Fig. 1C). ORF10 is almost entirely a β -strand structure, containing 34 strands and only 4 short helices (Fig. 1C). A detailed Dali server analysis revealed that the first and third domains of ORF10 form a fold resembling that of a monomeric dUTPase (deoxyuridine 5'-triphosphate pyrophosphatase) (*SI Appendix, Fig. S2A*). Thus, we refer to the first and third domains as dUTPase-L1 (dUTPase-like 1) and dUTPase-L2 (dUTPase-like 2), respectively. The second domain (denoted as the insertion domain) adopts a cylindrical β -barrel structure and protrudes out from the dUTPase region. Given that the monomeric dUTPases were reported to exist only in herpesviruses (29, 30), ORF10 may evolve from the herpesvirus dUTPase by gene duplication. Interestingly, unlike the typical dUTPases,

ORF10 does not contain a UTP-binding pocket (*SI Appendix, Fig. S2B*), and its potential catalytic residues are also not conserved (*SI Appendix, Fig. S2C*), indicating that ORF10 will play other roles beyond those of a dUTPase.

Interactions between ORF10 and the Rae1–Nup98 Heterodimer. The dimensions of the whole ORF10–Rae1–Nup98 complex are $\sim 97 \times 85 \times 50$ Å (*SI Appendix, Fig. S1A*). ORF10 forms two intermolecular interacting surfaces with the Rae1–Nup98 heterodimer (designated as interfaces I and II), which are mediated mainly by the extended CTT region (aa 403 to 418) and a loop (aa 58 to 62) of the dUTPase domain (Fig. 1C). The interacting sites on the Rae1–Nup98 heterodimer extend alongside blades 5 to 7 and reach back to blade 1 of the Rae1 β -propeller (Fig. 1D). Notably, ORF10 contacts the Rae1–Nup98 heterodimer primarily through Rae1 and forms hardly any notable interaction with Nup98, which is consistent with previous co-IP results showing that ORF10 forms a complex with Nup98 through Rae1 (25).

Interface I is an elongated intermolecular surface (~ 835 Å²) and is mediated by both hydrogen bonding and hydrophobic interactions between the CTT of ORF10 and blades 5 to 7 of the Rae1 β -propeller (Figs. 1D and 2A and B). Specifically, M413 of ORF10 inserts into a deep and compact hydrophobic pocket formed by blades 5 and 6 (F255, F257, W300, D301, K302, R305), suggesting an important anchor point between ORF10 and Rae1–Nup98 (Fig. 2B). It should be noted that M413 is highly conserved among different gammaherpesvirus ORF10 proteins (*SI Appendix, Fig. S3*), highlighting its potentially critical role. Several polar residues on ORF10 CTT (R403, E410, S411, E414, Q416) form additional hydrogen bonds with Rae1, further strengthening the interactions on interface I (Fig. 2A).

Unlike the elongated feature of interface I, interface II is a relatively compact surface (~ 304 Å²) (Fig. 1D). A protruding loop (aa 58 to 62) of the ORF10 dUTPase-L1 domain inserts into the cleft between blades 1 and 7 of the Rae1 β -propeller, forming both hydrogen bonding and hydrophobic interactions (Figs. 1D and 2C and D). Specifically, the highly conserved residue L60 of ORF10 (*SI Appendix, Fig. S3*) tightly packed within four hydrophobic residues of Rae1 (I32, V71, I329, L355) (Fig. 2D) highlights another important hydrophobic anchor point between ORF10 and Rae1–Nup98.

M413 and L60 of ORF10 Are Critical for Intermolecular Interactions with Rae1–Nup98. To evaluate the potential effects of the above intermolecular interactions, we generated multiple MHV-68 ORF10 mutations (detailed numbering is listed in *SI Appendix, Table S3*) on interface I (denoted as I_m1 to I_m9), interface II (II_m1 to II_m3), or both (I+II_m1 to I+II_m3) and tested their interactions with the Rae1–Nup98 complex using the co-IP method. Given the entire interface I is mediated by the CTT of ORF10, it is not surprising that CTT deletion mutants (I_m8: $\Delta 403$ to 418; I_m9: $\Delta 407$ to 418) completely abolish the interactions between ORF10 and Rae1–Nup98 (Fig. 3A). Similarly, the combined alanine substitutions of several critical amino acids within the CTT (I_m7: E410A/M413A/E414A/Q416A) also abolish the intermolecular interactions (Fig. 3A). To further validate the potential roles of single amino acids, we generated alanine substitutions of six residues of the CTT (I_m1: R403A; I_m2: D407A; I_m3: E410A; I_m4: M413A; I_m5: E414A; I_m6: Q416A) and performed the co-IP assays. Notably, M413A significantly reduces the binding between ORF10 and Rae1–Nup98, while other single-point mutations show only minimal reduction effects (Fig. 3A). Together, these results highlight the critical role of interface I and, particularly, the conserved residue M413 in the intermolecular interactions between ORF10 and Rae1–Nup98. Furthermore, we generated mutations of ORF10 on interface II and analyzed their effects for Rae1–Nup98 binding. A multiple-point mutant covering all residues of the interacting

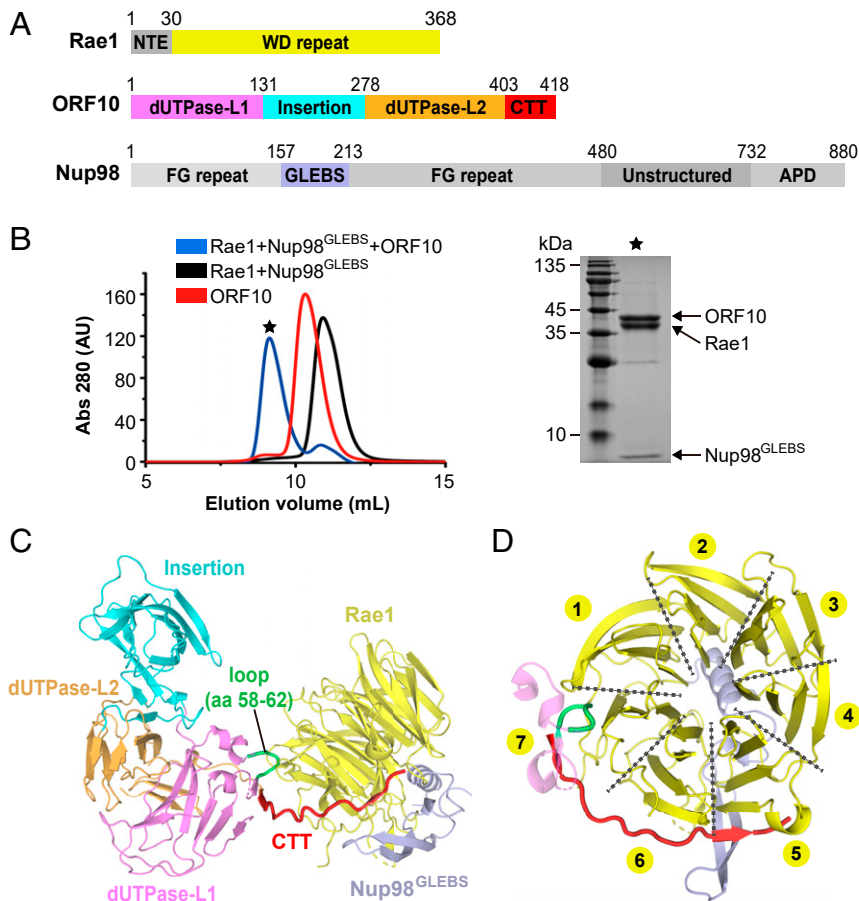


Fig. 1. Structure of the ORF10–Rae1–Nup98 ternary complex. (A) Domain organization of ORF10, Rae1, and Nup98. (B) Elution profiles of SEC runs on a Superdex 75 10/300 column that show the formation of the ORF10–Rae1–Nup98 complex (Left). The black star indicates the fraction analyzed by SDS/PAGE (Right). (C) Ribbon representation of the ORF10–Rae1–Nup98 complex, with the same color code as in A. Two regions of ORF10 that interact with Rae1–Nup98 are colored in green and red. (D) Top view of the Rae1 β -propeller highlighting the two interfaces between ORF10 and Rae1–Nup98.

loop in ORF10 (II_m1: H58A/G59A/L60A/S61A/E62A) practically abolishes the intermolecular contacts (Fig. 3B), confirming the critical role of interface II. Moreover, substitutions of the single residue L60 to either glutamic acid (II_m2: L60E) or serine (II_m3: L60S) disrupt the hydrophobic interactions of interface II and abolish the binding to Rae1–Nup98 (Fig. 3B). As expected, the mutants covering both interfaces, including both M413 and L60, also abolish the interactions (Fig. 3A). Given that M413 (on interface I) and L60 (on interface II) are important for intermolecular interactions and highly conserved among different gammaherpesvirus ORF10 proteins (*SI Appendix*, Fig. S3), we anticipated that these two sites would also play critical roles for other gammaherpesviruses in addition to MHV-68. In line with this hypothesis, co-IP assays show that both the single-point mutants and combined double mutants for L59 and M416 of KSHV ORF10 (equivalent sites of L60 and M413 in MHV-68 ORF10) practically abolish the interactions with Rae1–Nup98 (Fig. 3C), highlighting the critical and conserved roles of these two sites.

To confirm the co-IP results in a more direct context, we purified multiple MHV-68 ORF10 mutant proteins (for both interfaces I and II) by using the baculovirus–insect cell system and performed in vitro pull-down experiments for these mutants with the purified Rae1–Nup98 complex (Fig. 3D). Consistent with co-IP results, the mutants carrying M413, L60, or both significantly reduce the binding ability to Rae1–Nup98, while the mutants of other sites on both interfaces show only minimal

effects (Fig. 3D). Interestingly, both co-IP and in vitro pull-down results show that the mutations of ORF10 in one interface can almost block the interaction with Rae1 even though the other interface is wild type (WT). Thus, a stable interaction between ORF10 and Rae1 relies on the synergy contributions of both interfaces, and the loss of function of any interface will lead to the disruption of intermolecular interactions. Taken together, the co-IP and in vitro pull-down results confirm the intermolecular interactions found in the crystal structure and highlight the critical roles of M413- and L60-mediated hydrophobic interactions between ORF10 and Rae1–Nup98.

Interactions with Rae1–Nup98 Are Important for ORF10-Mediated mRNA Export Inhibition. The previous work does not provide a detailed understanding of the relationship between ORF10–Rae1–Nup98 interaction with ORF10-mediated RNA export inhibition (25). With our structural understanding, we next wanted to study the effects of intermolecular interactions on ORF10-mediated mRNA export inhibition. We employed a previously reported GFP expression plasmid as a reporter, which is sensitive to ORF10-mediated inhibition and carries the cytomegalovirus promoter and the simian virus 40 (SV40) early polyadenylation signal (25). Although wild-type MHV-68 ORF10 significantly down-regulates GFP expression (Fig. 4A and B), the loss-of-interaction mutants shown in the co-IP experiments (Fig. 3A and B) partially or completely rescue the inhibition (Fig. 4A and B). On the other hand, ORF10 mutants that only

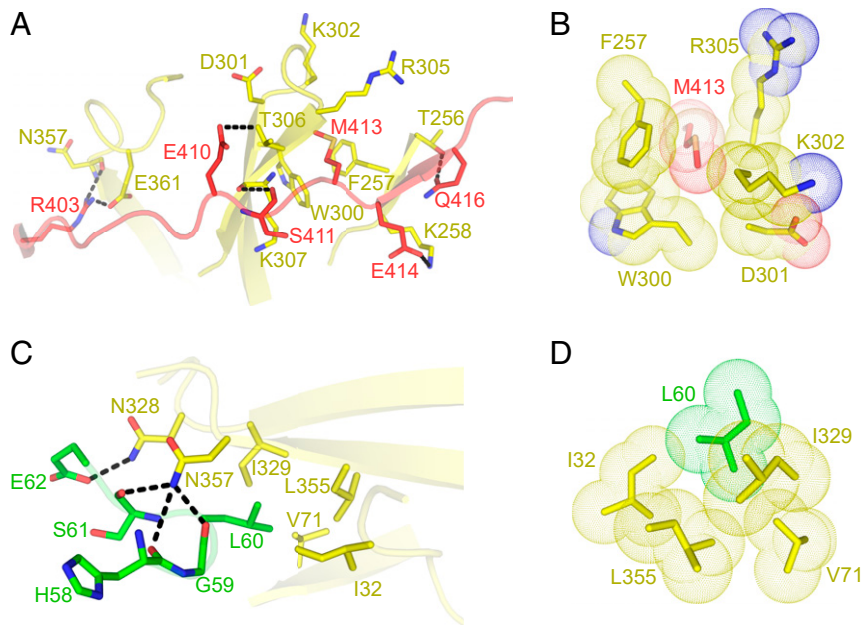


Fig. 2. Interactions between ORF10 and the Rae1–Nup98 heterodimer. (A) The residues involved in the interactions of interface I, with the hydrogen bonds shown as black dotted lines. Note that the CTT of ORF10 forms an elongated intermolecular surface with blades 5 to 7 of the Rae1 β -propeller. (B) Detailed hydrophobic interactions between M413 of ORF10-CTT and the residues F257/W300/D301/K302/R305 of Rae1. (C) The residues involved in the interactions of interface II, with the hydrogen bonds shown as black dotted lines. Note that loop 58 to 62 of ORF10 inserts into the cleft between blades 1 and 7 of the Rae1 β -propeller. (D) Detailed hydrophobic interactions between L60 of the ORF10 dUTPase-L1 domain and residues I32/V71/I329/L355 of Rae1.

slightly affect the interactions show minimal rescue abilities (Fig. 4A and B). In line with the MHV-68 ORF10 results, mutants of KSHV ORF10 reduce the efficiency of mRNA export inhibition (Fig. 4A and B) to a degree similar to the reduction for the Rae1–Nup98 interaction (Fig. 3C). To evaluate the GFP expression levels in a more accurate manner, we conducted FACS (fluorescence-activated cell sorting) assays for several critical ORF10 mutants to quantify the percentage of GFP-positive cells and the geometric mean of fluorescence intensity. Consistent with the confocal microscopy experiments (Fig. 4A and B), the FACS-based results also reveal that the mutants show reductions for ORF10-mediated GFP expression inhibition at a level similar to their disruptions of the Rae1–Nup98 interaction (Fig. 3A–C and *SI Appendix*, Fig. S4A and B).

To confirm that the inhibition of GFP expression is due to the reduction of mRNA export, we measured the nuclear to cytoplasmic (Nu/Cy) ratio of GFP transcripts by extracting the nuclear and cytoplasmic fractions. As shown in Fig. 4C and D, the expression of wild-type ORF10 from both MHV-68 and KSHV causes a significant increase in the Nu/Cy ratio of GFP transcripts. However, the loss-of-interaction ORF10 mutants fail to retain GFP mRNA in the nucleus (Fig. 4C and D). It should be noted that the nuclear and cytoplasmic fractionation efficiency has been rigorously evaluated by three different markers, including the nuclear U6 RNA (*SI Appendix*, Fig. S5A), the nuclear protein LaminaA/C (*SI Appendix*, Fig. S5B and C), and the cytoplasmic protein GAPDH (*SI Appendix*, Fig. S5B and C). Moreover, we also monitored the poly(A)⁺ RNA distribution by using a previously reported *in situ* oligo(dT) hybridization method (25). As expected, wild-type ORF10 proteins from both MHV-68 and KSHV result in a decrease in cytoplasmic poly(A)⁺ RNA signal with a concomitant increase in nuclear labeling, while the loss-of-interaction ORF10 mutants fail to do so (*SI Appendix*, Fig. S6A and B). Taken together, these results reveal that the binding between ORF10 and Rae1–Nup98 is critical for the inhibition of mRNA export and that the disruption of intermolecular interactions will rescue this inhibition.

ORF10 and M Protein Share a Similar Binding Site on Rae1–Nup98. It is known that the M protein of VSV also interacts with the Rae1–Nup98 complex and prevents export of bulk mRNAs during VSV infection (15, 17, 23, 24). Structural superimposition of ORF10–Rae1–Nup98 and M–Rae1–Nup98 complexes shows that these two viral proteins share no structural similarity and bind to opposite sides of the Rae1–Nup98 complex (Fig. 5A). Unexpectedly, the N-terminal tail (NTT) of the M protein and the CTT of ORF10 bind within the same groove of Rae1–Nup98 and share a similar conformation of the main chains (Fig. 5A). This groove carries an overall positive electrostatic potential surface and can be perfectly fitted by the overall negatively charged NTT of the M protein or CTT of ORF10 (Fig. 5A and *SI Appendix*, Fig. S7A and B). Notably, ORF10-CTT forms a more extended interacting surface with Rae1–Nup98 than that of the M NTT (Fig. 5A). Moreover, the critical methionine (M413) of the ORF10 CTT and the intermolecular hydrophobic interactions mediated by this residue are also conserved in the M–Rae1–Nup98 complex (Fig. 5B). Together, these results show that the Rae1–Nup98 complex is a common target by different viruses and its positively charged groove is a critical binding site for two completely different viral proteins.

RNA-Binding Ability of ORF10 Is Important for mRNA Export Inhibition. The positively charged groove that both ORF10 and the M protein bind in has been reported to be the single-stranded RNA (ssRNA) binding region of Rae1–Nup98 (17, 23), and the formation of the M–Rae1–Nup98 ternary complex disrupts its RNA-binding ability (23). We initially anticipated that ORF10–Rae1–Nup98 would also lose the RNA-binding ability in a way similar to M–Rae1–Nup98. However, electrophoretic mobility shift assays (EMSAs) reveal that ORF10–Rae1–Nup98 maintains a RNA-binding ability comparable to Rae1–Nup98 (Fig. 5C and D). Given that the original RNA interacting groove of Rae1–Nup98 has been occupied by the CTT of ORF10, the existing RNA-binding ability of ORF10–Rae1–Nup98 may be contributed by ORF10. Consistent with this

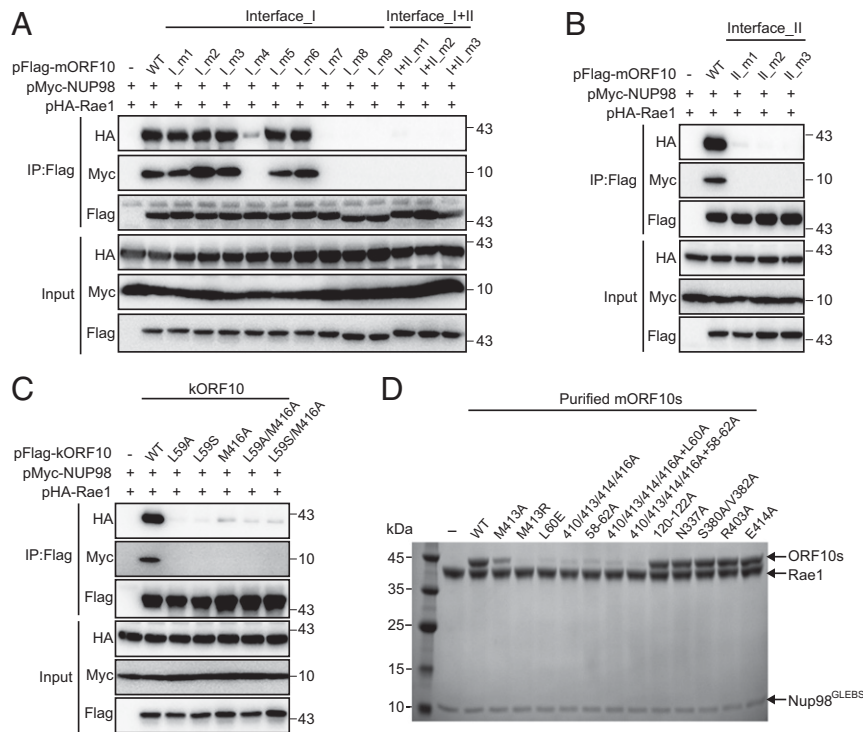


Fig. 3. L60 (interface I) and M413 (interface II) of ORF10 play a critical and conserved role for interacting with Rae1–Nup98. (A and B) Coimmunoprecipitation analysis to show the interactions between Rae1–Nup98 and MHV-68 ORF10 carrying indicated mutations (detailed numbering is listed in *SI Appendix, Table S2*). (C) Coimmunoprecipitation analysis to show the interaction between Rae1–Nup98 and KHSV ORF10 carrying indicated mutations. (D) In vitro pull-down analysis between Rae1–Nup98 (His-tag) and different MHV-68 ORF10 proteins (no tag). Note that the ORF10 mutants containing L60 and/or M413 mutations significantly reduce the intermolecular binding.

hypothesis, the purified ORF10 protein indeed binds RNA in a concentration-dependent manner (Fig. 5E). ORF10 also contributes to the RNA-binding ability in the presence of the Rae1–Nup98 complex (Fig. 5F). Furthermore, ORF10 (or the ORF10–Rae1–Nup98 complex) has similar binding affinities with poly(U) (Fig. 5C and E) and poly(A) (*SI Appendix, Fig. S8A and B*) oligos. In line with our in vitro direct RNA-binding results, the previous RNA–IP experiments also show that the ORF10-bound Rae1–Nup98 complex still associates with RNA transcripts (25). Taken together, these results reveal that although ORF10 occupies a RNA-binding surface of Rae1–Nup98 similar to that of the M protein, the ORF10–Rae1–Nup98 ternary complex can still interact with RNA through ORF10.

Electrostatic surface potential calculation reveals that ORF10 contains three separated positively charged regions (denoted as regions I, II, and III), as shown in Fig. 6A–C. It should be noted that none of these three potential RNA-binding regions overlap with the Rae1–Nup98 interacting interfaces (interfaces I and II). To check which region is critical for the ORF10-mediated inhibition of mRNA export, we designed multiple mutations for the positively charged residues in all three regions (*SI Appendix, Table S4*) and employed the GFP reporter system to validate their effects on mRNA export (Fig. 6D and E). Confocal microscopy results show that the mutants in region I, but not regions II and III, significantly reduce the inhibition of mRNA export (Fig. 6D and E and *SI Appendix, Table S4*), suggesting a critical role of this surface in RNA binding and RNA export inhibition. As expected, the EMSA result shows that the RNA-binding affinity of the region I_m2 mutant (*SI Appendix, Fig. S8C*) is much weaker than that of the wild-type ORF10 (Fig. 5E). Furthermore, the in situ oligo(dT) hybridization assays confirm that only the region I mutant, not region II and III mutants, reduces ORF10-mediated nuclear accumulation of poly(A)⁺

RNA (*SI Appendix, Fig. S9A and B*). Together, our results demonstrate that ORF10 employs a unique mechanism to inhibit the RNA export of host cells and its RNA-binding ability is critical for this inhibition.

Discussion

Viruses possess sophisticated strategies to hijack or impair host mRNA nuclear export pathways, thereby facilitating the export of viral transcripts and preventing the host cells from setting up a proper antiviral environment. Among the previously identified viral proteins targeting mRNA export processes, so far, ORF10 represents the only example that inhibits a selective subset of host transcripts rather than bulk inhibition (25). Moreover, ORF10 also represents the first viral protein of the *Herpesviridae* family that can inhibit host mRNA export (25). Thus, detailed research of ORF10-mediated inhibition, shown in the current work, is essential to understand the diversity of viral inhibition of mRNA nuclear export and provide potential therapeutic targets for viral infections.

Our structure confirms that ORF10 contains a monomeric dUTPase domain, although the sequence similarities between ORF10 and typical dUTPase are very low. The three-dimensional architecture of ORF10 is important for its interactions with Rae1–Nup98, as it brings the two separated regions (aa 58 to 62 and aa 403 to 418) of ORF10 into a structurally closed conformation and makes them accessible to the binding sites of Rae1. It should be noted that these two Rae1-binding surfaces of ORF10 are not among the mostly conserved regions, although the two critical amino acids (L60 and M413) are highly conserved. Thus, it is difficult to predict the potential Rae1-binding sites of ORF10 based on only sequence alignment (*SI Appendix, Fig. S3*). Three other relatively conserved regions (120 to 122, 337, 380/382) have been predicted to participate in Rae1

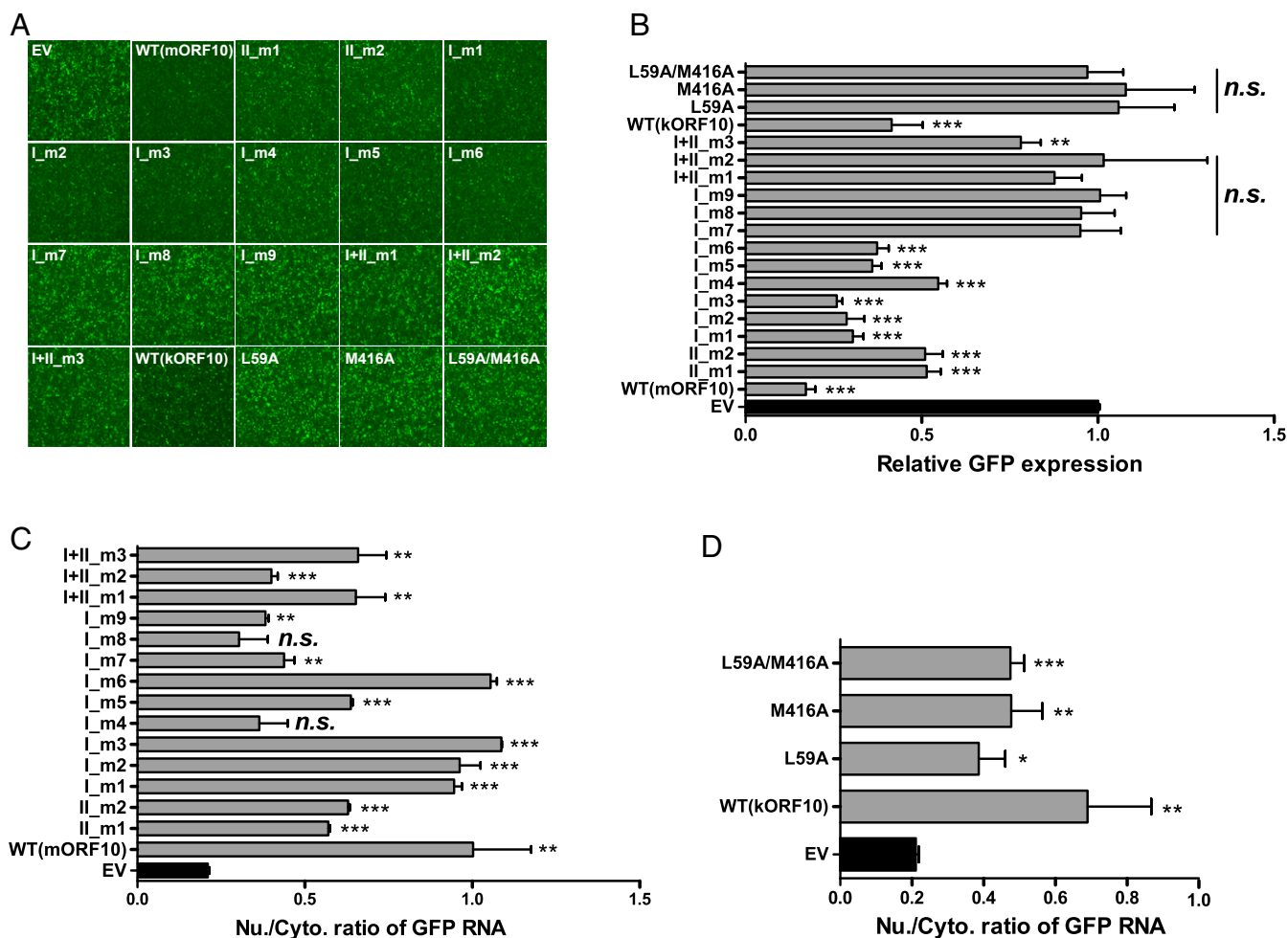


Fig. 4. Interactions with Rae1–Nup98 are important for ORF10-mediated mRNA export inhibition. (A) The effects of mutations of ORF10 (from both MHV-68 and KSHV) on the GFP expression were analyzed by fluorescence microscopy. (B) Quantification of the fluorescence intensity in A with ImageJ. Data are mean \pm SD and representative of three independent biological replicates. Student's *t* test, n.s., not significant; ****P* < 0.01, *****P* < 0.001. (C and D) The cytoplasm and nuclear RNAs were extracted from transfected cells in A, and the GFP transcript was quantified by qRT-PCR. The Nu/Cy ratio of the GFP transcript is plotted as mean \pm SD (*n* = 3). Student's *t* test, n.s., not significant; **P* < 0.05, ****P* < 0.01, *****P* < 0.001. EV, empty vector.

interaction, and alanine substitutions of these regions indeed affect the ORF10-mediated mRNA export inhibition (25). However, the current ORF10–Rae1–Nup98 structure shows that these three regions are far from the interacting surfaces (Figs. 1 and 2). Moreover, our *in vitro* pull-down experiments show that mutations of these regions do not reduce the interactions with Rae1–Nup98 (Fig. 3D). Thus, rather than directly participate in binding to Rae1–Nup98, these three conserved regions of ORF10 may contribute to other steps of mRNA export inhibition.

Despite extensive studies over many years, the precise functions of Rae1 and the Rae1–Nup98 complex are still unclear. It has been proposed that Rae1 may both promote the recruitment of the major export factor NXF1 to Nup98 (11–17) and facilitate the transport of a specific subset of mRNAs by itself (25). Interestingly, ORF10 and the M protein, two completely different proteins from unrelated virus families, both target the Rae1–Nup98 complex and inhibit its function, highlighting a potentially critical role of Rae1–Nup98 in regulating mRNA trafficking and in setting up a proper antiviral cellular condition. Although ORF10 and the M protein bind to opposite sides of Rae1–Nup98, they both occupy the RNA-binding groove of Rae1–Nup98. Thus, both ORF10 and the M protein should be able to inhibit the nuclear export of the specific subset of mRNAs regulated by Rae1–Nup98

itself. However, only ORF10 shows a selective inhibition of mRNA export (25), while the M protein nonspecifically prevents export of bulk mRNAs (15, 24). One possibility for this difference is that the M protein may interfere with both the RNA-binding ability of Rae1–Nup98 and the recruitment of NXF1 to Nup98; in contrast, ORF10 may inhibit only the RNA binding of Rae1–Nup98 and not the NXF1 recruitment. Moreover, although ORF10 has been found to selectively block nuclear export of a subset of mRNAs based on their 3' UTRs (25), it is still unclear whether ORF10 and the ORF10–Rae1–Nup98 complex recognize specific RNA sequences or certain higher-order RNA structures. Clearly, further studies will be needed to reveal these unresolved questions. Nevertheless, these two viral proteins with different inhibition mechanisms can be used as important tools to study the precise functions of Rae1.

An interesting feature of ORF10-mediated RNA export inhibition is that the ORF10–Rae1–Nup98 ternary complex can still associate with RNA due to the RNA-binding ability of ORF10, although ORF10 occupies the intrinsic RNA-binding groove of Rae1–Nup98. Conversely, the M–Rae1–Nup98 complex entirely loses its RNA-binding ability. Our functional results show that mutations on ORF10's RNA-binding surface abolish its inhibition for mRNA export, revealing a direct connection between RNA binding and RNA export inhibition. Previous work shows that

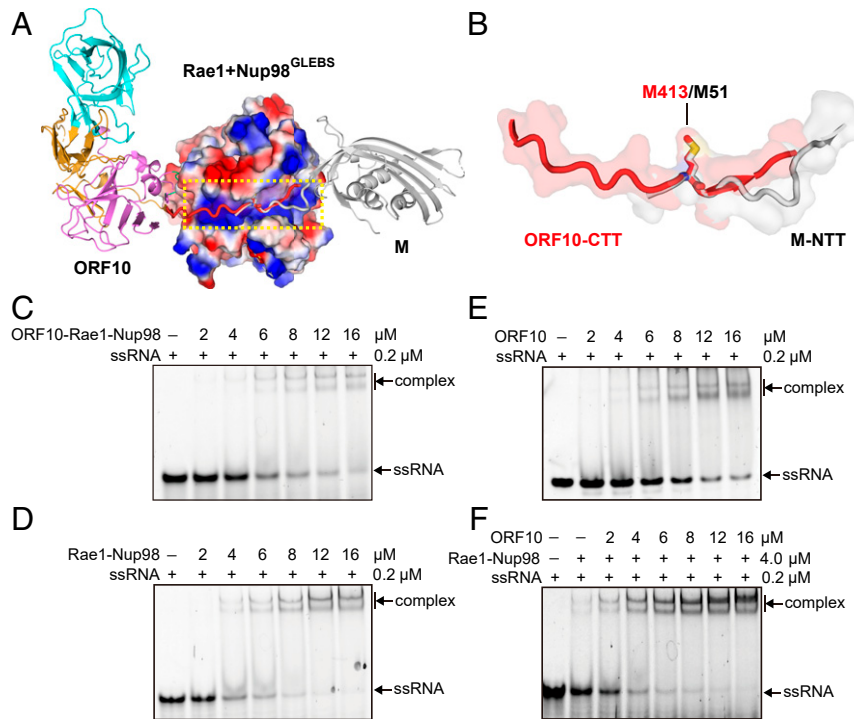


Fig. 5. ORF10 utilizes a unique mechanism to inhibit mRNA export. (A) Structural superposition between ORF10–Rae1–Nup98 (same color code as in Fig. 1C) and M–Rae1–Nup98 (silver; PDB ID code: 4OWR). The Rae1–Nup98 heterodimer was shown in the electrostatic potential surface representation. (B) CTT of ORF10 (red) and NTT of the M protein (silver) occupy a similar surface of Rae1–Nup98. The two well-superimposed methionine residues are shown by a stick. (C–F) EMSA assays showing the binding between FAM-labeled poly(U) ssRNA and indicated proteins in variant concentrations. The bands were visualized by fluorescence of FAM.

knocking down of Rae1 changes the cellular distribution of ORF10 from nuclear envelope to cytoplasm (25). It is likely that ORF10 translocates to the nuclear envelope by interacting with Rae1–Nup98 and then accesses and binds to a specific subset of mRNAs

based on their 3' UTRs, thereby preventing the nuclear export of this subset of transcripts.

In summary, our work reveals detailed structural and molecular mechanisms of ORF10-mediated inhibition of mRNA

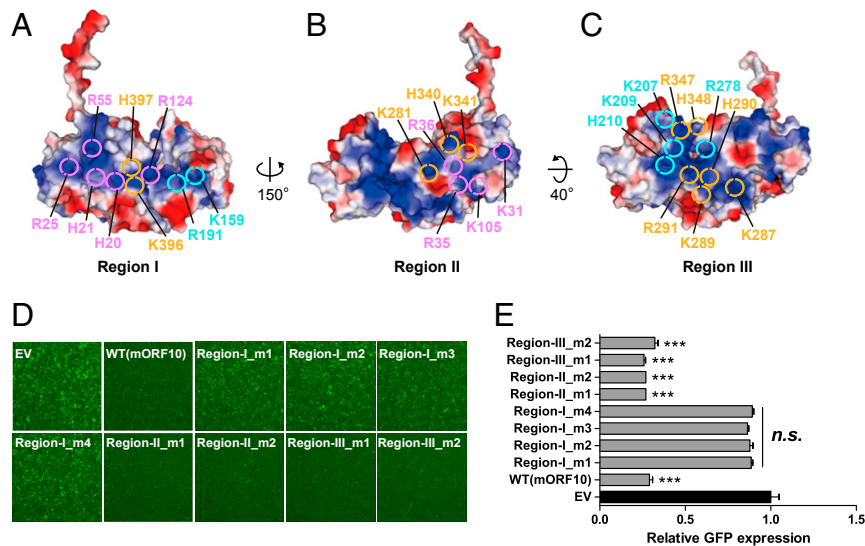


Fig. 6. Mutations on the RNA-binding surface disrupt ORF10-mediated mRNA export inhibition. (A–C) Electrostatic potential surface representation of ORF10 in three different views. The positively charged residues in regions I (A), II (B), and III (C) are highlighted by circles. Different colors indicate that these residues belong to different domains (same color code as in Fig. 1A). (D) GFP expression in cells cotransfected with MHV-68 ORF10 WT or mutants of positively charged residues in A–C was analyzed by fluorescence microscopy. (E) Quantification of fluorescence intensity in D with ImageJ. Data are mean \pm SD ($n = 3$). Student's t test, n.s., not significant; *** $P < 0.001$. EV, empty vector.

nuclear export and serves as an important reference to elucidate the functions of the Rae1–Nup98 complex.

Materials and Methods

Plasmid Construction. The gene encoding MHV-68 ORF10 was synthesized and codon optimized for expression in Sf9 cells. The genes encoding RNA export 1 (Rae1) and the Gle2-binding sequence (GLEBS) motif of Nup98 (residues 157 to 213) were amplified by PCR using mouse peripheral blood complementary DNA (cDNA) as the template. Different ORF10 constructs were inserted into the BamHI and HindIII restriction sites of a modified pFastBac Dual vector (Invitrogen) that contains a Tobacco Etch Virus (TEV)-cleavable N-terminal His tag. Mouse Nup98 GLEBS motif and Rae1 were cloned into the same modified pFastBac Dual vector (Invitrogen) at the first expression site (BamHI, HindIII) with a TEV-cleavable N-terminal His tag and the second expression site (XhoI, KpnI) without a tag, respectively. In addition, pCMV-Flag-ORF10 (both MHV-68 and KSHV), pCMV-HA-Rae1, and pCMV-Myc-Nup98^{GLEBS} plasmids were constructed and used for co-IP and immunofluorescence experiments. All point mutants and truncations were prepared from the full-length constructs by PCR.

Protein Expression and Purification. All of the recombinant proteins were expressed in Sf9 cells (Invitrogen). The Rae1–Nup98^{GLEBS} complex was prepared by using a coexpression strategy, while ORF10 was separately expressed. Sf9 cells were infected with the recombinant baculovirus and grown in suspension at 27 °C for 3 d. The cells were harvested by centrifugation (2,000 × g, 4 °C, 10 min). The cell pellets were resuspended and lysed by ultrasonication in lysis buffer containing 50 mM Tris (pH 7.5), 500 mM NaCl, 10 mM imidazole, 2 mM β-mercaptoethanol (β-ME), and 1 mM phenylmethanesulfonyl fluoride (PMSF). All of the recombinant proteins were first purified by Ni²⁺ affinity chromatography. The supernatant was loaded onto the Ni²⁺ column; then the protein was eluted with 50 mM Tris (pH 7.5), 500 mM NaCl, 250 mM imidazole, and 2 mM β-ME. The N-terminal His tags of both ORF10 and the Rae1–Nup98^{GLEBS} complex were removed by TEV protease digestion. The proteins were then loaded onto a Superdex 200 10/300 GL gel filtration column (GE Healthcare) equilibrated with the storage buffer containing 20 mM Tris (pH 7.5), 200 mM NaCl, and 1 mM DL-dithiothreitol (DTT). To prepare the ORF10–Nup98^{GLEBS} ternary complex, equimolar amounts of ORF10 and Rae1–Nup98^{GLEBS} heterodimer proteins were mixed and purified via size exclusion chromatography in the storage buffer. The purified ORF10–Rae1–Nup98^{GLEBS} ternary complex was concentrated to ~20 mg/mL and stored at –80 °C. The ORF10 mutants were expressed and purified following the same protocol used for the wild-type protein.

Crystallization and Structure Determination. Crystals of the ORF10–Rae1–Nup98 complex were grown at 20 °C by the sitting drop vapor diffusion method. The crystallization screen was performed by mixing 1 μL protein solution and 1 μL reservoir solution. The final crystallization condition was 0.2 M disodium tartrate, 20% polyethylene glycol 3350 (pH 7.5). The heavy-atom derivative crystals were obtained by soaking native crystals in the crystallization solution containing 5 mM ethylmercurithiosalicylic acid (sodium salt) for 1 h at 20 °C.

Diffraction data sets were collected at 100 K on the BL19U beamline of Shanghai Synchrotron Radiation Facility. Then the data were indexed, integrated, and scaled using the HKL program suite (31). The structure was solved by the single-wavelength anomalous dispersion method using anomalous X-ray diffraction data obtained from a Hg derivative by the PHENIX software package (32). The rest of the model was manually built using COOT (33). The refinement was carried out using PHENIX (32). The statistics of data collection and refinement are shown in *SI Appendix, Table S1*. Structural figures were prepared using Pymol.

In Vitro Pull-Down Assays. The purified His-tagged Rae1–Nup98 complex was incubated with 20 μL Ni Sepharose beads (GE Healthcare) for 30 min at 16 °C and washed three times with the binding buffer (20 mM Tris-HCl, pH 7.5; 200 mM NaCl; 10 mM imidazole). The purified wild-type and mutant ORF10 proteins were added to the protein-coated beads for 30 min at 16 °C. Then beads were washed extensively with the buffer containing 20 mM Tris-HCl (pH 7.5), 200 mM NaCl, and 20 mM imidazole. The bound proteins were eluted using the buffer containing 20 mM Tris-HCl (pH 7.5), 200 mM NaCl, and 250 mM imidazole and analyzed by sodium dodecyl sulfate/polyacrylamide gel electrophoresis (SDS/PAGE).

Electrophoretic Mobility Shift Binding Assays. The high performance liquid chromatograph grade 10-mer poly(U) ssRNA was synthesized with the 5' FAM label in GenScript. The ssRNA oligo was incubated with increasing concentrations of the Rae1–Nup98 binary complex, the ORF10–Rae1–Nup98 ternary complex, or ORF10 alone in a buffer containing 20 mM Tris (pH 8.0), 150 mM NaCl, and 5% (vol/vol) glycerol for 10 min at room temperature. The final concentrations of ssRNA and protein samples (Rae1–Nup98, ORF10–Rae1–Nup98, or ORF10) in a 10 μL mixture were 0.2 and 0 to 16 μM, respectively. The reaction samples were loaded on a 6% native PAGE gel in the Tris-borate-EDTA buffer (45 mM Tris, pH 8.5, buffer titrated with boric acid). The ssRNA was visualized using the fluorescence signal from the FAM label. To further confirm ORF10's contribution to RNA binding, ORF10 samples in different concentrations (0 to 16 μM) were added to the preincubated mixture of ssRNA (0.2 μM) and the Rae1–Nup98 complex (4 μM) and incubated for 20 min at room temperature. The samples were loaded on the native PAGE gel and visualized by fluorescence signal of FAM using the same protocol shown above. EMSA experiments for the 10-mer poly(A) ssRNA and ORF10 (or ORF10–Rae1–Nup98 complex) were performed following the same protocol used for the poly(U) ssRNA.

co-IP and Western Blot. 293T cells in 6 cm dishes were transfected with Rae1, Nup98, and ORF10 (WT and mutants). After 24 to 36 h posttransfection, cells were lysed in cell lysis buffer (50 mM Tris-HCl, pH 8.0; 150 mM NaCl; 1% Triton X-100 plus mixture and phenylmethylsulfonyl fluoride [PMSF]) for 30 min at 4 °C. Five percent of the cell lysate was taken as input, and the remainder was immunoprecipitated with appropriate antibody agarose for 5 h at 4 °C. Immunoprecipitates were washed with cell lysis buffer five times and boiled in SDS/PAGE loading buffer for Western blotting. Samples were separated with SDS/PAGE and transferred to poly vinylidene fluoride membranes (Merck Millipore). After blocking in PSB containing 0.1% Tween-20 and 5% skim milk, the blots were probed with indicated antibodies.

Poly(A) mRNA In Situ Hybridization. Poly(A) mRNA in situ hybridization was performed using a method described previously (25) with some modifications. Briefly, transfected cells were fixed with 4% paraformaldehyde for 10 min, then followed by the addition of 100% cold methanol for 10 min. The methanol was aspirated, and cells were rehydrated in 70% ethanol for 15 min. Cells were then rinsed in 1 M Tris (pH 8.0) for 5 min, followed by prehybridization in hybridization buffer (1 mg/mL yeast transfer RNA, 0.005% bovine serum albumin, 10% dextran sulfate, 25% formamide in 2XSSC [saline sodium citrate] buffer) for 60 min at 37 °C, then hybridized with the Cy3-labeled oligo(dT) probe (1 ng/μL in hybridization buffer) overnight at 37 °C. After hybridization, cells were washed once with 4XSSC and three times in 2XSSC. Subsequent indirect immunofluorescence was performed with the primary Flag antibody (in 2XSSC, 0.1% Triton X-100) for 2 h at room temperature, then incubated with Alexa Fluor 488–conjugated secondary antibody (in 2XSSC, 0.1% Triton X-100) for 1 h. Cells were washed three times with 2XSSC, and then DNA was stained with DAPI for 10 min. Slides were analyzed by ZEISS LSM 700.

Nuclear and Cytoplasmic RNA Fractionation. Nuclear and cytoplasmic RNA fractionation was extracted according to a method described previously with modifications (25). Briefly, 293T cells in 12-well plates were harvested by trypsinization and further washed with cold diethyl pyrocarbonate-treated phosphate buffer saline three times. Then, cells were pelleted at 1,500 rpm for 3 min at 4 °C, resuspended in 1 mL of re-suspended buffer (RSB) buffer (10 mM Tris, pH 7.4; 10 mM NaCl; 3 mM MgCl₂; 1 mM DTT), and incubated on ice for 5 min, followed by centrifugation at 1,500 rpm for 3 min. The cell pellet was resuspended by pipetting with 100 μL lysis buffer RSBG40 buffer (10 mM Tris, pH 7.4; 10 mM NaCl; 3 mM MgCl₂; 10% glycerol; 0.5% Nonidet P-40; 1 mM DTT). The nuclei were pelleted at 1,500 rpm for 5 min. The supernatant was saved as the cytoplasmic fraction and centrifuged twice at 13,000 rpm for 10 min at 4 °C to remove any nuclei or cellular debris. The nuclei were resuspended with 1 mL RSBG40D buffer by gently pipetting, incubated on ice for 5 min, and then pelleted at 1,500 rpm for 3 min. After washing with RSBG40D buffer three times, the nuclei were collected as the nuclear fraction. RNA of cytoplasmic and nuclear fractions was extracted with TRIzol reagent (Life Technology) following the manufacturer's instructions.

Reverse Transcription and Real-Time PCR. RNA reverse transcription (RT) was performed according to Genomic DNA Eraser Reverse Transcription Kits (Takara, catalog no. RR047A). Briefly, 1 μg of RNA was treated with DNA eraser, and then cDNA was synthesized using PrimeScript RT enzyme mix

and RT primer mix. To determine the GFP RNA transcript copy number, 100 ng RNA were subjected to real-time PCR.

Fluorescence Microscopy and Flow Cytometry. 293T cells in 12-well plates were transfected with pEGFP-C1 and ORF10 mutants. After 36 h posttransfection, samples were examined with fluorescence microscopy (Olympus CKX41). Then, cells were harvested by trypsinization, and GFP positive cells were analyzed using FACS Calibur (BD).

Reagents and Cells.

Reagents. The reagents were Dulbecco's Modified Eagle's medium (DMEM) (Gibco by Thermo Fisher Scientific, catalog no. C11965500BT), fetal bovine serum (Biological Industries, catalog no. 04-001-1ACS), Anti-FLAG M2 Affinity Gel (Merck, catalog no. A2220), anti-Flag antibody (Sigma-Aldrich, F7425), anti-HA antibody (Sigma-Aldrich, H6908), anti-Myc antibody (Sigma-Aldrich, catalog no. SAB4300319), and anti-HA agarose (Merck, catalog no. A2095).

Cells. HEK-293T cells were cultured in DMEM supplemented with 10% fetal bovine serum and 1% penicillin–streptomycin. iSLK-219 cells were maintained

in the presence of 1 μ g/mL puromycin, 250 μ g/mL G418, and 1 μ g/mL hygromycin B.

Data Availability Statement. The atomic coordinates and the related experimental data have been deposited in the Protein Data Bank (PDB) (PDB ID code 7BYF). The materials are also available from the corresponding author upon request.

ACKNOWLEDGMENTS. We thank the staff of the BL17B1, BL18U1, and BL19U1 beamlines at the National Center for Protein Sciences Shanghai and Shanghai Synchrotron Radiation Facility, Shanghai, China, for assistance during data collection. We thank Dr. Ang Gao for the critical reading and helpful discussion. This work was supported by grants from the National Key R&D Program of China (Grants 2018YFA0507203 and 2018YFA0508000), the National Natural Science Foundation of China (Grants 31922037, 81921005, 31670903, 31900872, 31900131, and 81325012), the Chinese Academy of Sciences (KJZD-SW-L05, XDB37030203, and XDB37030205), and the Youth Innovation Promotion Association (Grant 2020093).

1. H. Cheng *et al.*, Human mRNA export machinery recruited to the 5' end of mRNA. *Cell* **127**, 1389–1400 (2006).
2. M. Delaleau, K. L. Borden, Multiple export mechanisms for mRNAs. *Cells* **4**, 452–473 (2015).
3. A. J. Shatkin, J. L. Manley, The ends of the affair: Capping and polyadenylation. *Nat. Struct. Biol.* **7**, 838–842 (2000).
4. S. R. Carmody, S. R. Wenthe, mRNA nuclear export at a glance. *J. Cell Sci.* **122**, 1933–1937 (2009).
5. M. Müller-McNicoll, K. M. Neugebauer, How cells get the message: Dynamic assembly and function of mRNA-protein complexes. *Nat. Rev. Genet.* **14**, 275–287 (2013).
6. G. M. Hautbergue, M. L. Hung, A. P. Golovanov, L. Y. Lian, S. A. Wilson, Mutually exclusive interactions drive handover of mRNA from export adaptors to TAP. *Proc. Natl. Acad. Sci. U.S.A.* **105**, 5154–5159 (2008).
7. I. C. Braun, A. Herold, M. Rode, E. Izaurralde, Nuclear export of mRNA by TAP/NXF1 requires two nucleoporin-binding sites but not p15. *Mol. Cell Biol.* **22**, 5405–5418 (2002).
8. N. G. Farny, J. A. Hurt, P. A. Silver, Definition of global and transcript-specific mRNA export pathways in metazoans. *Genes Dev.* **22**, 66–78 (2008).
9. A. Bachi *et al.*, The C-terminal domain of TAP interacts with the nuclear pore complex and promotes export of specific CTE-bearing RNA substrates. *RNA* **6**, 136–158 (2000).
10. S. K. Kuss, M. A. Mata, L. Zhang, B. M. A. Fontoura, Nuclear imprisonment: Viral strategies to arrest host mRNA nuclear export. *Viruses* **5**, 1824–1849 (2013).
11. M. B. Blevins, A. M. Smith, E. M. Phillips, M. A. Powers, Complex formation among the RNA export proteins Nup98, Rae1/Gle2, and TAP. *J. Biol. Chem.* **278**, 20979–20988 (2003).
12. S. M. Bailer *et al.*, Nup116p and nup100p are interchangeable through a conserved motif which constitutes a docking site for the mRNA transport factor gle2p. *EMBO J.* **17**, 1107–1119 (1998).
13. A. Bharathi *et al.*, The human RAE1 gene is a functional homologue of *Schizosaccharomyces pombe* rae1 gene involved in nuclear export of Poly(A)⁺ RNA. *Gene* **198**, 251–258 (1997).
14. J. A. Brown *et al.*, A mutation in the *Schizosaccharomyces pombe* rae1 gene causes defects in poly(A)⁺ RNA export and in the cytoskeleton. *J. Biol. Chem.* **270**, 7411–7419 (1995).
15. P. A. Faria *et al.*, VSV disrupts the Rae1/mrnp41 mRNA nuclear export pathway. *Mol. Cell* **17**, 93–102 (2005).
16. C. E. J. Pritchard, M. Fornerod, L. H. Kasper, J. M. A. van Deursen, RAE1 is a shuttling mRNA export factor that binds to a GLEBS-like NUP98 motif at the nuclear pore complex through multiple domains. *J. Cell Biol.* **145**, 237–254 (1999).
17. Y. Ren, H. S. Seo, G. Blobel, A. Hoelz, Structural and functional analysis of the interaction between the nucleoporin Nup98 and the mRNA export factor Rae1. *Proc. Natl. Acad. Sci. U.S.A.* **107**, 10406–10411 (2010).
18. M. L. Yarbrough, M. A. Mata, R. Sakthivel, B. M. A. Fontoura, Viral subversion of nucleocytoplasmic trafficking. *Traffic* **15**, 127–140 (2014).
19. N. Satterly *et al.*, Influenza virus targets the mRNA export machinery and the nuclear pore complex. *Proc. Natl. Acad. Sci. U.S.A.* **104**, 1853–1858 (2007).
20. L. Zhang *et al.*, Inhibition of pyrimidine synthesis reverses viral virulence factor-mediated block of mRNA nuclear export. *J. Cell Biol.* **196**, 315–326 (2012).
21. Y. Qiu, R. M. Krug, The influenza virus NS1 protein is a poly(A)-binding protein that inhibits nuclear export of mRNAs containing poly(A). *J. Virol.* **68**, 2425–2432 (1994).
22. K. Zhang *et al.*, Structural basis for influenza virus NS1 protein block of mRNA nuclear export. *Nat. Microbiol.* **4**, 1671–1679 (2019).
23. B. Quan, H. S. Seo, G. Blobel, Y. Ren, Vesiculoviral matrix (M) protein occupies nucleic acid binding site at nucleoporin pair (Rae1•Nup98). *Proc. Natl. Acad. Sci. U.S.A.* **111**, 9127–9132 (2014).
24. J. P. Rodrigues *et al.*, Vesicular stomatitis virus matrix protein inhibits host cell gene expression by targeting the nucleoporin Nup98. *Mol. Cell* **6**, 1243–1252 (2000).
25. D. Gong *et al.*, A herpesvirus protein selectively inhibits cellular mRNA nuclear export. *Cell Host Microbe* **20**, 642–653 (2016).
26. L. A. Johnson, L. Li, R. M. Sandri-Goldin, The cellular RNA export receptor TAP/NXF1 is required for ICP27-mediated export of herpes simplex virus 1 RNA, but the TREX complex adaptor protein Aly/REF appears to be dispensable. *J. Virol.* **83**, 6335–6346 (2009).
27. L. A. Johnson, R. M. Sandri-Goldin, Efficient nuclear export of herpes simplex virus 1 transcripts requires both RNA binding by ICP27 and ICP27 interaction with TAP/NXF1. *J. Virol.* **83**, 1184–1192 (2009).
28. M. D. Koffa *et al.*, Herpes simplex virus ICP27 protein provides viral mRNAs with access to the cellular mRNA export pathway. *EMBO J.* **20**, 5769–5778 (2001).
29. N. Tarbouriech, M. Buisson, J. M. Seigneurin, S. Cusack, W. P. Burmeister, The monomeric dUTPase from Epstein-Barr virus mimics trimeric dUTPases. *Structure* **13**, 1299–1310 (2005).
30. L. Freeman *et al.*, The flexible motif V of Epstein-Barr virus deoxyuridine 5'-triphosphate pyrophosphatase is essential for catalysis. *J. Biol. Chem.* **284**, 25280–25289 (2009).
31. Z. Otwinowski, W. Minor, Processing of X-ray diffraction data collected in oscillation mode. *Methods Enzymol.* **276**, 307–326 (1997).
32. P. D. Adams *et al.*, PHENIX: A comprehensive python-based system for macromolecular structure solution. *Acta Crystallogr. D Biol. Crystallogr.* **66**, 213–221 (2010).
33. P. Emsley, B. Lohkamp, W. G. Scott, K. Cowtan, Features and development of coot. *Acta Crystallogr. D Biol. Crystallogr.* **66**, 486–501 (2010).